Electronic Supplementary Information (ESI)

for

Stable cross-linked lyotropic gyroid mesophases from single-tail/single-head cross-linkable monomers

Omar Q. Imran,[a,b] Patrick Li,[c] Na Kyung Kim,[b] Douglas L. Gin[c] and Chinedum O. Osuji*[b]

a. Department of Chemical and Environmental Engineering, Yale University, New Haven, CT 06510, USA

b. Department of Chemical and Biomolecular Engineering, University of Pennsylvania, Pennsylvania, PA 19104, USA

c. Department of Chemistry, University of Colorado, Boulder, CO 80309, USA.

Materials

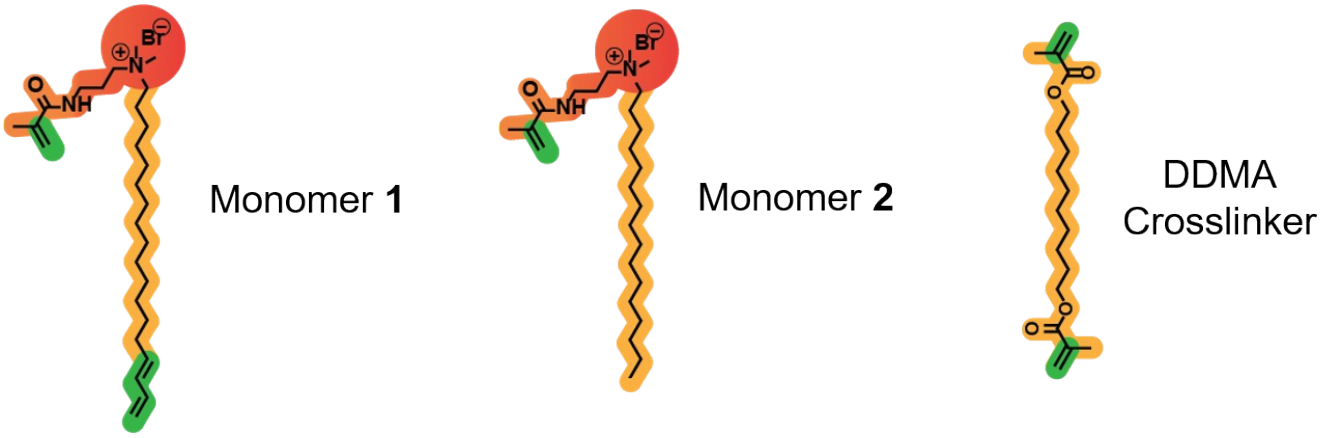

Fig. S1 Chemical structures of intrinsically cross-linkable monomer **1**, non-cross-linkable monomer **2**, and commercial cross-linker DDMA. (red/orange = hydrophilic headgroup region, yellow = hydrophobic tail region, green = polymerizable site)

Synthesis of Monomers 1 and 2

Chromium (IV) oxide, pyridine, *tert*-butyl lithium (1.6 M in pentane), hydrogen bromide (48% wt. % in H_2O), borane-tetrahydrofuran complex solution (1.0 M in THF), *ω*-pentadecalactone (98%), sulfuric acid, triethanolamine (98%), *N*-3-(dimethylamino)propylmethacrylamide, 3,5-di-*tert*-4-butylhydroxytoluene, 1-bromohexadecane (97%), and Florisil® (<200 mesh) were purchased from the Sigma-Aldrich Chemical Co. and used as received unless otherwise specified. *N,N,N′,N′,*-tetramethylethylenediamine (98%), allyltrimethylsilane (98%), and 2-isopropoxy-4,4,5,5-tetramethyl-1,3,2-dioxaborolane (98%) were purchased from TCI America and used as received unless otherwise specified. Aluminum oxide (neutral, act. I, 50–200 µm) and silica gel (normal-phase, 200 x 400 mesh) were purchased from Sorbent Technologies. Sodium chloride, magnesium sulfate, Celite™ 545, and hydrochloric acid (all ACS Reagents) were purchased from Fisher Scientific and used as received. All solvents were obtained from the Sigma-Aldrich Chemical Co. and were purified/dehydrated via vacuum distillation and then de-gassed by repeated freeze-pump-thaw cycles and stored under Ar. All chemical syntheses were carried out under a dry Ar atmosphere using standard Schlenk line techniques unless otherwise noted.

NMR spectra were obtained using a Bruker Avance-III 300 NMR spectrometer (300 MHz for ^{1}H, 75 MHz for ^{13}C). Chemical shifts are reported in parts per million relative to the solvent residual signal (DMSO, δ_H = 2.50 ppm, δ_C = 39.52 ppm). FTIR spectra (neat) were recorded on an Agilent Cary 630 FTIR instrument single-reflection horizontal ATR accessory with diamond crystal. Elemental analysis was performed by Galbraith Laboratories, Inc.

(E)-*N*-(3-methacrylamidopropyl)-*N*,*N*-dimethyloctadeca-15,17-dien-1-aminium bromide (monomer 1)

18-Bromooctadeca-1,3-diene (1.9979 g, 6.0658 mmol, 1.0000 equiv.), *N*-3-(dimethylamino)propylmethacrylamide (1.1360 g, 6.6725 mmol, 1.1000 equiv.), and 3–4 crystals of 3,5-di-*tert*-4-butylhydroxytoluene were dissolved in CH_3CN (10 mL) in a 25-mL amber Schlenk flask equipped with a stir bar. The solution was stirred at 70 °C for 24 h in the dark. The contents of the Schlenk flask were cooled to room temperature and precipitated from Et_2O (200 mL) in a Dry Ice-acetone bath. The precipitate was filtered immediately and dried in vacuo to give monomer **1** as a white solid (2.6491 g, 87%).

^{1}H NMR (300 MHz, DMSO-d_6): δ 8.06 (t, *J* = 5.8 Hz, 1H), 6.39 – 6.20 (m, 1H), 6.11 – 5.96 (m, 1H), 5.79 – 5.65 (m, 1H), 5.67 (td, *J* = 1.9, 1.0 Hz, 1H), 5.35 (p, *J* = 1.6 Hz, 1H), 5.15 – 5.02 (m, 1H), 5.01 – 4.90 (m, 1H), 3.21 (ddd, *J* = 19.0, 9.7, 4.9 Hz, 6H), 2.99 (s, 6H), 2.03 (q, 1H), 1.86 (dd, *J* = 1.6, 0.9 Hz, 3H), 1.61 (s, 2H), 1.39 – 1.21 (m, 14H). ^{13}C NMR (75 MHz, DMSO-d_6): δ 167.64, 139.75, 137.23, 135.29, 130.88, 119.28, 115.09, 62.84, 50.12, 35.91, 31.88, 29.03, 28.99, 28.85, 28.60, 28.58, 28.52, 25.77, 22.46, 21.65, 18.61. FTIR (neat): 3224, 2917, 2849, 1656, 1619, 1531, 1467, 1318, 1212, 1070, 1003, 912, 803, 720 cm^{-1}. Calc. for $C_{27}H_{51}BrN_2O$: C, 64.91; H, 10.29; N, 5.61. Found: C, 64.68; H, 10.26; N, 5.58.

***N*-(3-Methacrylamidopropyl)-*N*,*N*-dimethylhexadecan-1-aminium bromide (monomer 2)**

1-Bromohexadecane (8.0000 g, 0.026200 mol, 1.0000 equiv.), *N*-3-(dimethylamino)propylmethacrylamide (4.9068 g, 0.028821 mol, 1.1000 equiv.), and 3–4 crystals of 3,5-di-*tert*-4-butylhydroxytoluene were dissolved in CH_3CN (50 mL) in a 100-mL amber Schlenk flask equipped with a stir bar. The solution was stirred at 70 °C for 24 h in the dark. The contents of the Schlenk flask were cooled to room temperature and precipitated from Et_2O (200 mL) in a Dry Ice-acetone bath. The precipitate was filtered immediately and dried in vacuo to give monomer **2** as a white solid (8.1317 g, 65%).

^{1}H NMR (300 MHz, DMSO-d_6): δ 8.08 (t, *J* = 5.8 Hz, 1H), 5.69 (dd, *J* = 1.5, 0.9 Hz, 1H), 5.35 (p, *J* = 1.5 Hz, 1H), 3.30 – 3.11 (m, 6H), 3.00 (s, 6H), 1.93 – 1.76 (m, 4H), 1.61 (s, 2H), 1.24 (s, 25H), 0.91 – 0.80 (m, 3H). ^{13}C NMR (75 MHz, DMSO-d_6): δ 167.63, 139.73, 119.27, 62.84, 60.90, 50.12, 35.90, 31.27, 29.04, 28.99, 28.94, 28.80, 28.69, 28.51, 25.77, 22.43, 22.08, 21.64, 18.60, 13.94. FTIR (neat): 3378, 2918, 2850, 1653, 1612, 1530, 1465, 1334, 1220, 1067, 970, 923, 809, 720 cm^{-1}. Calc. for $C_{25}H_{51}BrN_2O$: C, 63.14; H, 10.81; N, 5.89. Calc. for $C_{25}H_{53}BrN_2O_2 \bullet H_2O$: C, 60.83; H, 10.82; N, 5.68. Found: C, 60.82; H, 10.75; N, 5.68.

The newly synthesized monomers are hygroscopic, ionic organic compounds that are difficult to dry completely and usually do not combust well. However, their obtained elemental analysis values are within the accepted ±0.4% tolerance range for C, H, and N to be considered pure when the presence of associated water molecules is accounted for.[1]

Other Mesophase Additives

All other materials used in mesophase formulation were purchased from Sigma-Aldrich and used as received. A cross-linker additive 1,10-decanediol dimethacrylate (DDMA) was used for a mesophase formulation discussed in Fig. 3a. The standard radical photo-initiator used for most mesophase formulations was 2,2-dimethoxy-2-phenylacetophenone (DMPA); but for the data discussed in Fig. S4 2-hydroxy-4'-(2-hydroxyethoxy)-2-methylpropiophenone (HHMP) was the photo-initiator used for mesophase formulation instead of DMPA.

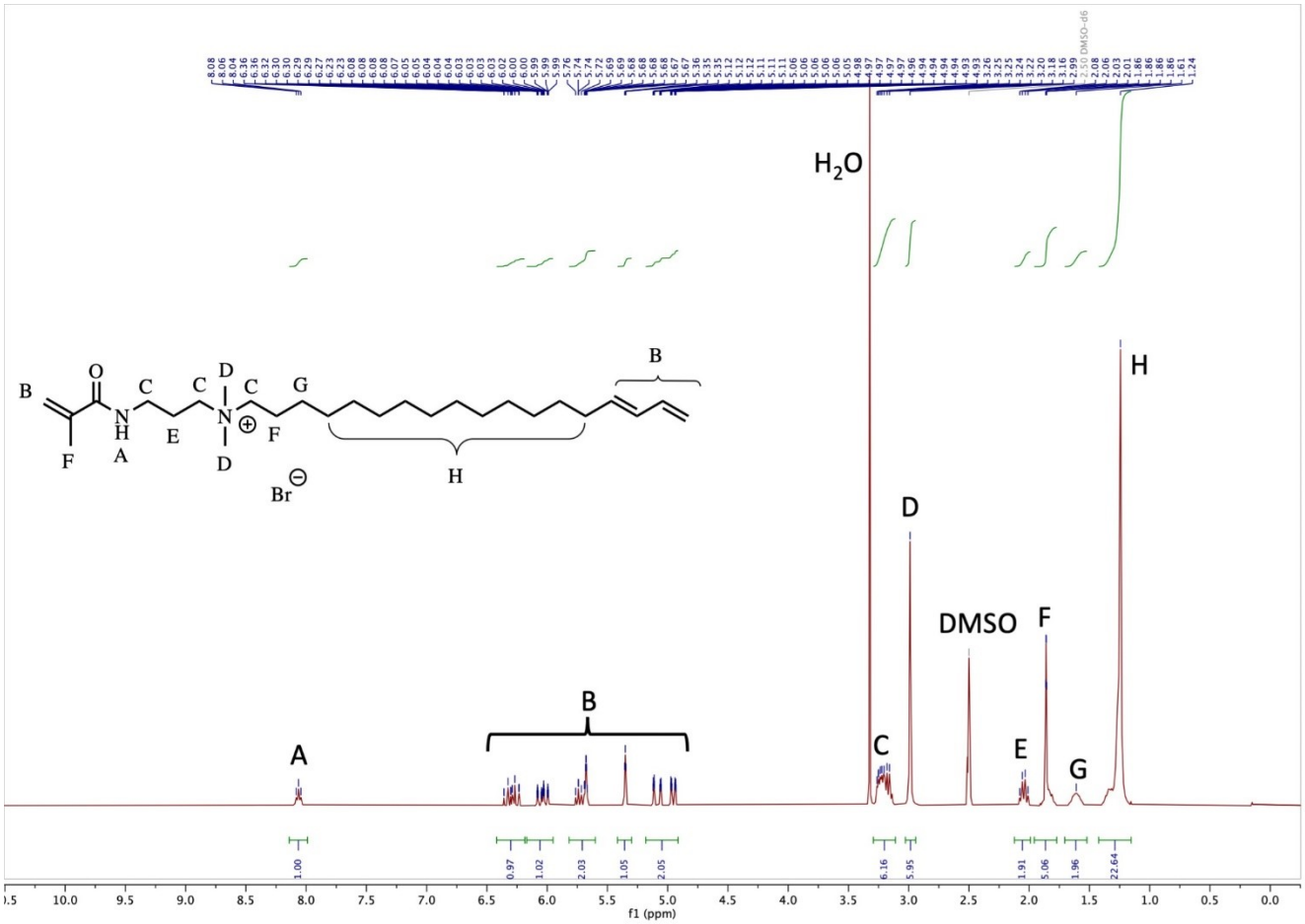

Fig. S2 ^{1}H NMR spectrum of monomer **1** in DMSO-d_6

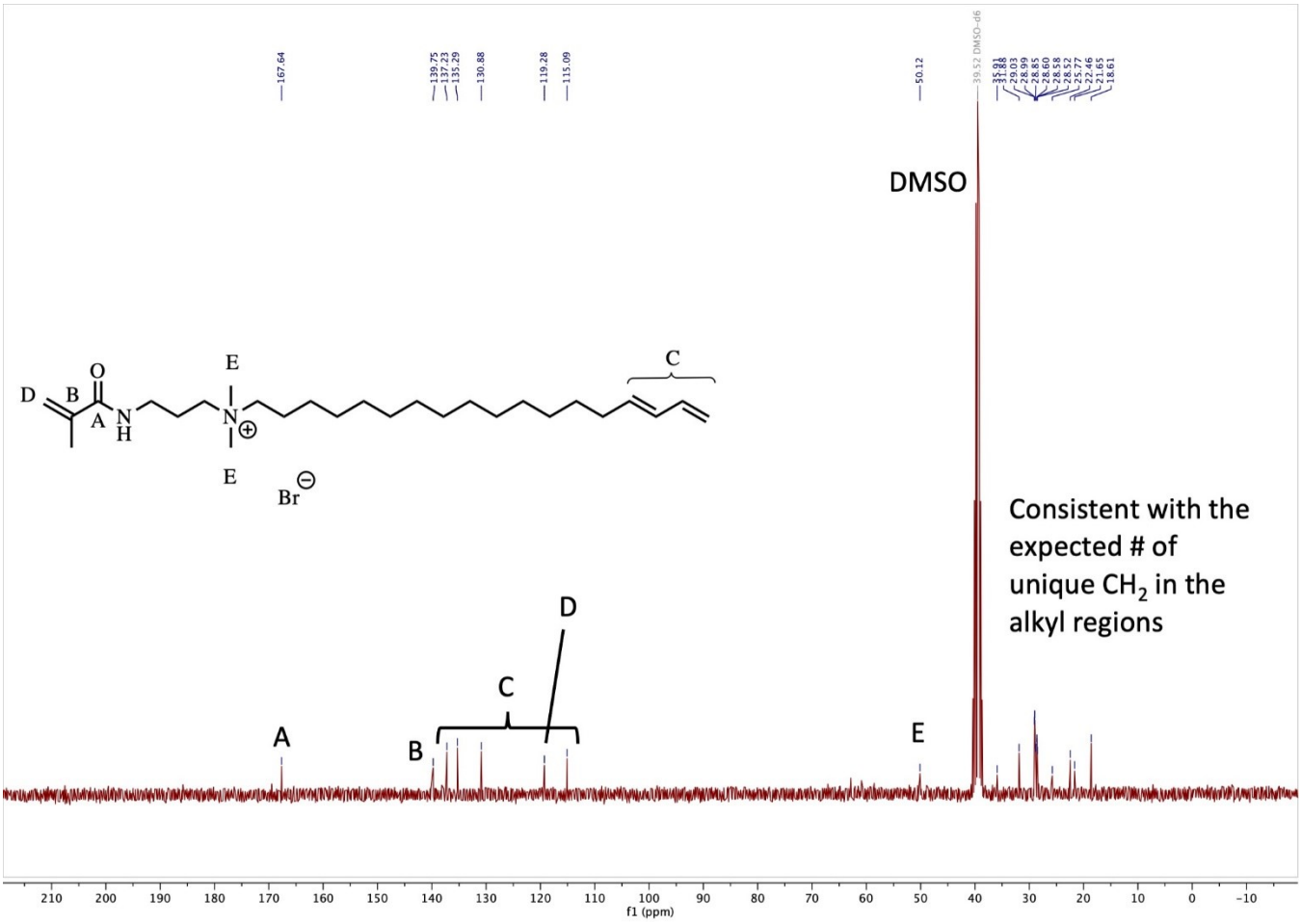

Fig. S3 ^{13}C NMR spectrum of monomer **1** in DMSO-d_6

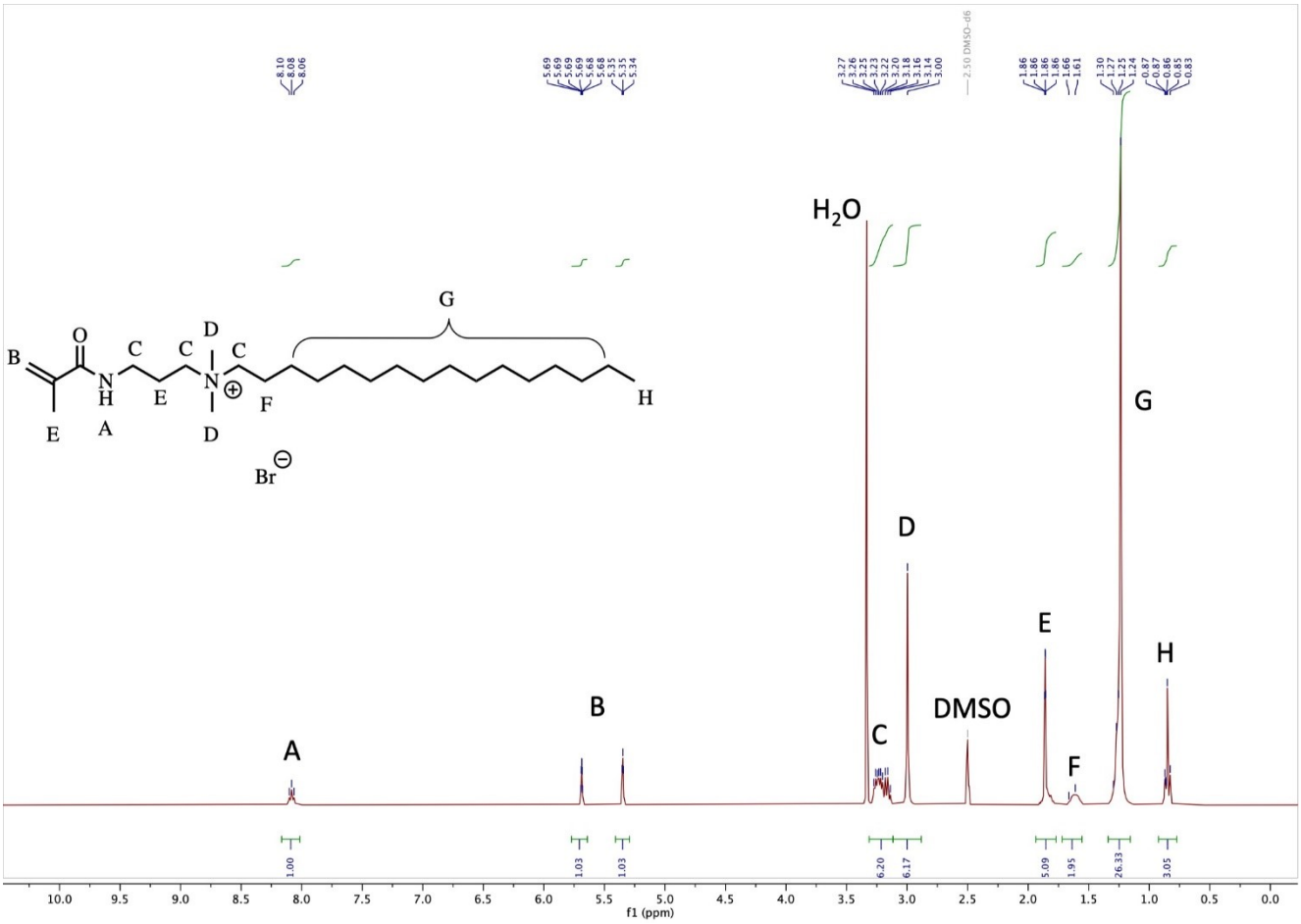

Fig. S4 ^{1}H NMR spectrum of monomer **2** in DMSO-d_6

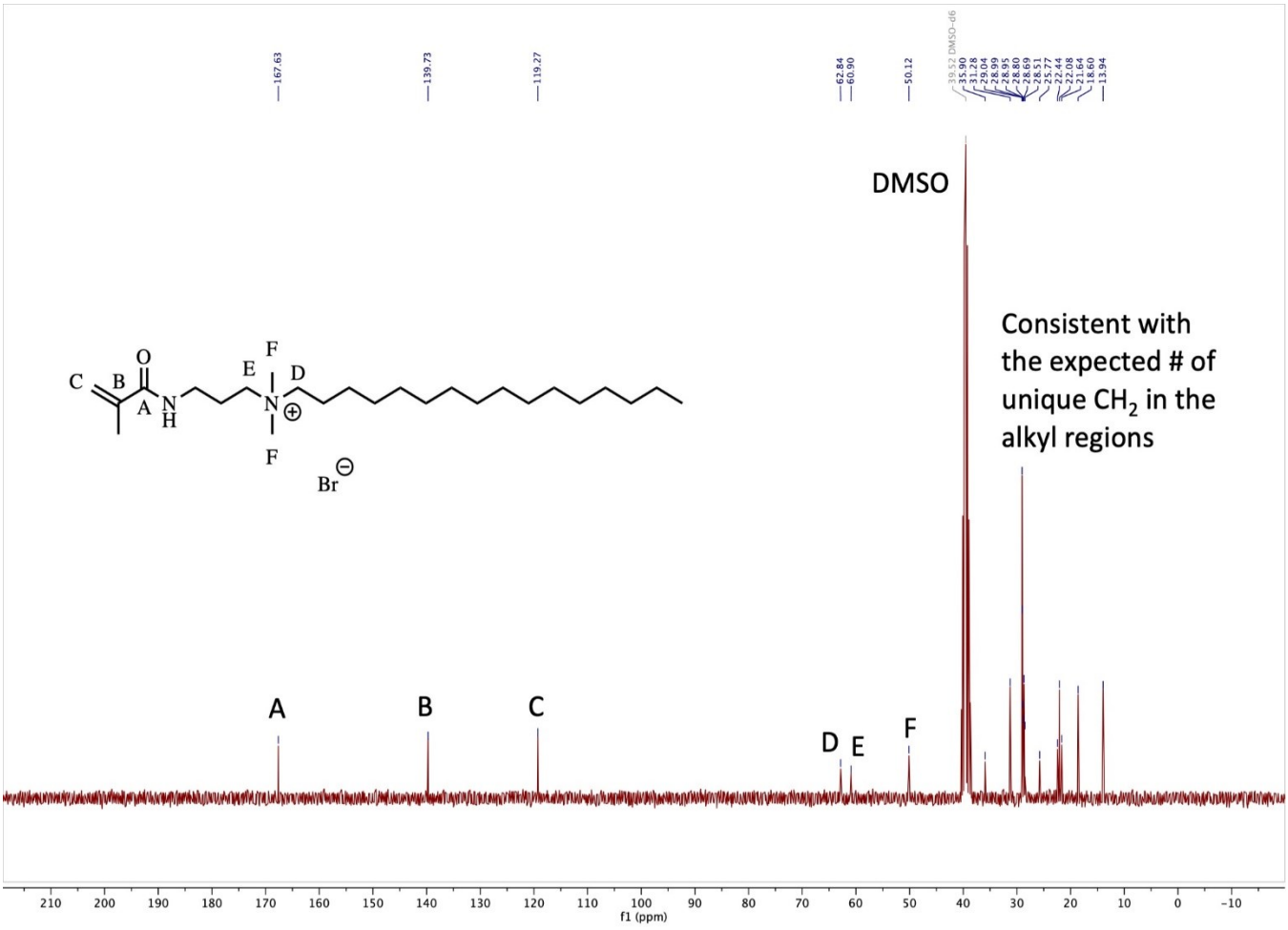

Fig. S5 ^{13}C NMR spectrum of monomer **2** in DMSO-d_6

Methods

Mesophase Compositions

Table S1 Compositions of the double-gyroid mesophases

Sample	Monomer (wt%)	Water (wt%)	DMPA (wt%)	DDMA cross-linker (wt%)
Monomer **1,** gyroid phase (base case)	87.5	11.5	1	0
Monomer **2,** gyroid phase	88	11	1	0
Monomer **2** + DDMA, gyroid phase	84	11	1	4

General Mesophase Formulation Procedure

In a 1.5-mL microcentrifuge tube, 100 µL of DMPA solution (1 wt% DMPA in ethyl acetate) were pipetted. The solvent was evaporated via vacuum, leaving ca. 1 mg DMPA initiator coated on the vial walls and base. Monomer powder (typically 87.5 mg) was measured into the vial, after which 11.5 µL of water were pipetted into the vial, for a total of 100 mg of vial contents.

The tubes at were centrifuged at 14500 rpm for ca. 1 h. After the centrifugation, the tubes were left in a 70 °C drying oven in the dark for 2 min, after which the contents of the tubes were manually mixed with a blunt needle. After these steps, the tubes were returned to the centrifuge for another 1 hour run at the same speed. This sequence of steps was repeated 2–4 times until a uniformly transparent, high-viscosity gyroid monomer mesophase was formed in the centrifuge tubes, possessing a highly-viscous 'gel-like' consistency.

Polymer Film Fabrication Procedure

20–50 mg of the gyroid monomer mesophase was sandwiched between two clean glass slides, and then pressed until the mesophase spread to a sufficiently large area (typically > 4 cm^2). On occasion a bench/shop vise was used to spread the high viscosity mesophase over a sufficiently large area between the glass slides.

The samples were placed in a chamber with nitrogen purge and UV-crosslinked by exposure to a beam from a 100-W Sunspot SM system. The lamp emission spectrum is distributed in the wavelength range between 250–450 nm, with the peak intensity at 365 nm. After UV exposure for 3 h, cross-linked gyroid films were obtained between the glass slides. A razor blade was used to remove sections of the polymer gyroid films from the glass substrate. The risk of water evaporation during this long-duration polymerization is minimized by the 'sandwiching' of the monomer mesophase between glass slides, which prevents the majority of the material from coming into contact with an evaporation surface. Further, the

lack of observed phase change under POM (Fig. 2) in the polymer film (i.e., gyroid to lamellar or crystal), combined with the very minor difference in SAXS traces of mesophase and polymer (Fig. 2), indicate that any evaporation has a negligible effect on the nanostructure during the long polymerization.

Polarized Optical Microscopy (POM)

The unpolymerized monomer mesophase and the corresponding polymerized films were observed under crossed-polarizers using a Zeiss Axiovert 200 M inverted microscope with a CCD camera accessory connected to a computer.

Small-Angle X-Ray Scattering (SAXS)

SAXS were measured using a Xenocs Xeuss 2.0 system in the Dual Source and Environmental X-ray Scattering (DEXS) facility at the University of Pennsylvania. A GeniX3D Cu source with a wavelength of λ = 1.54 Å was used, with a typical sample to detector distance of 37.5 cm providing a range of accessible scattering vectors (q) from 0.016 to 1.4 $Å^{-1}$. Silver behenate was used as a standard for calibrating the sample-to-detector distance. Both monomer mesophase and polymer film samples were packed between Kapton windows. Foxtrot software was used for azimuthal integration of scattering patterns into 1-D plots of scattering intensity (I) versus q. The lattice parameter a of the double-gyroid unit cell was calculated from the q-values of the (211) peaks in the 1D plots via the relation $a = (2\pi\sqrt{6})/q$. For temperature-dependent SAXS measurements, a polymer film was placed on a Linkam heating stage (Model Number L-HFSX350). The stage was heated from 30 °C to 210 °C with a heating scan rate of 10 °C/min, and X-ray spectra were obtained at every 15 °C within the temperature range.

Fourier-transform Infrared (FTIR) Spectroscopy

FTIR spectra (neat) were recorded using an Agilent Cary 630 FTIR instrument single-reflection horizontal ATR accessory with diamond crystal.

Charged Dye Solute Adsorption Experiments

Gyroid polymer films (approximately 1 cm^2 in area) with weights ranging from 5.0 to 9.6 mg were immersed in 40-mL volumes of aqueous dye solutions and shaken on a laboratory vortex mixer for 72 h to encourage dye uptake. The following aq. concentrations were used for the various dyes: Methylene Blue (15 μM), Methyl Orange (15 μM), Rose Bengal (15 μM), and Reactive Red 120 (75 μM). After 72 h, the polymer films were removed from the dye solutions and photographed. The percent change in the absorbances of the dye solutions at the 0- and 72-h marks were measured from a Cary 300 UV-Vis spectrophotometer operated in transmission mode using a dual-beam configuration.

Uncharged Solute Filtration Experiments

A thick gyroid film (*ca.* 100 μm) was installed in a high-pressure stirred cell (HP4750 Stirred Cell). Active membrane area was *ca.* 2 cm^2 (membrane diameter of 1.6 cm). An aqueous Vitamin B12 feed solution (0.05 wt%, 369 μM) was permeated through the membrane at an applied pressure of ca. 500 psig (ca. 35 bar). The first 1 mL of permeate was discarded, and the second 1 mL was collected for measurement. VB12 rejection was quantified by the absorbance differences measured between feed and permeate solutions with a Cary 300 UV-Vis spectrophotometer.

Supplementary Data

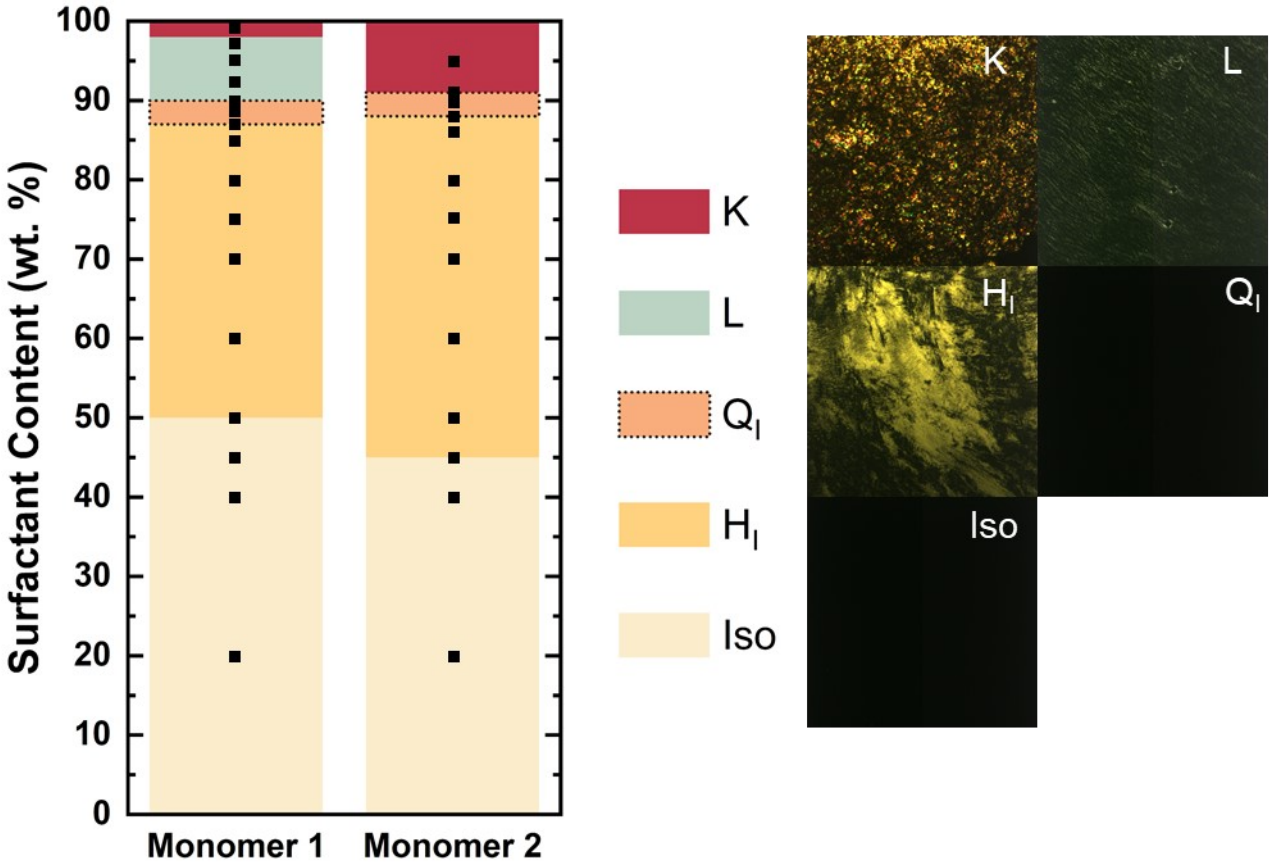

Fig. S6 Binary phase diagrams of aqueous mixtures of monomer **1** and of monomer **2** at room temperature (22–25 °C), as approximately determined from POM analysis. Typical POM textures for micellar/isotropic (Iso), normal hexagonal (H_I), normal bicontinuous cubic (Q_I), lamellar (L), and crystal phases (K) are shown. (Note: The H and Q phases observed for monomer **1** + water were assigned as Type I (i.e., normal) phases based on their position on the water-excessive side of an observed central L phase (see Ref. 1 in the main manuscript).) On occasion, coexistence of phases was observed at the estimated phase boundaries. Black squares indicate compositions where mesophase determination was made via POM.

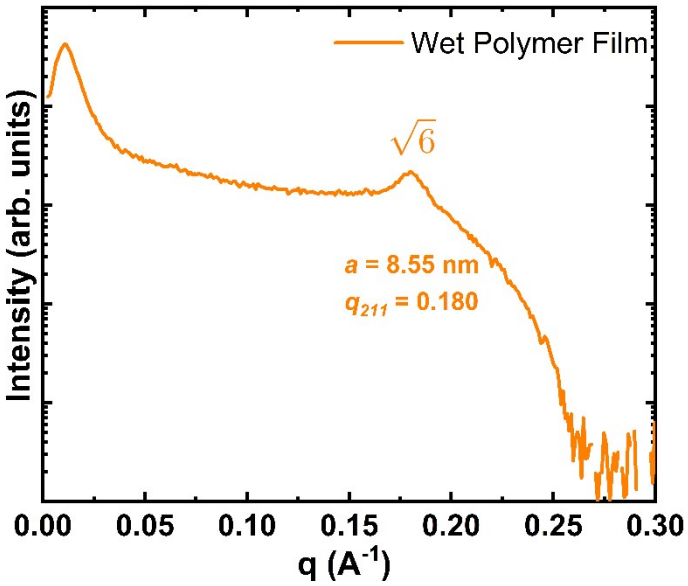

Fig. S7 SAXS spectrum of a wet polymer film of **1** under non-vacuum conditions from a secondary (different q-range; lower-resolution) instrument (Rigaku SMAX-3000). The SAXS data were collected with the sample cavity filled with water. Due to the i) lower power and ii) shorter q-range of the non-vacuum instrument ($q < 0.22$ A^{-1}), as well as iii) the intensity attenuation from the presence of water in the sample holder, the (220) peak expected at $q = 0.208$ A^{-1} cannot be discerned. However, the lattice parameter of the wet film (a = 8.55 nm) was unchanged relative to the lattice parameter reported for a dry film in Figure 2 of the manuscript (a = 8.55 nm). This invariance of the structure indicates that water immersion does not significantly swell the gyroid polymer network.

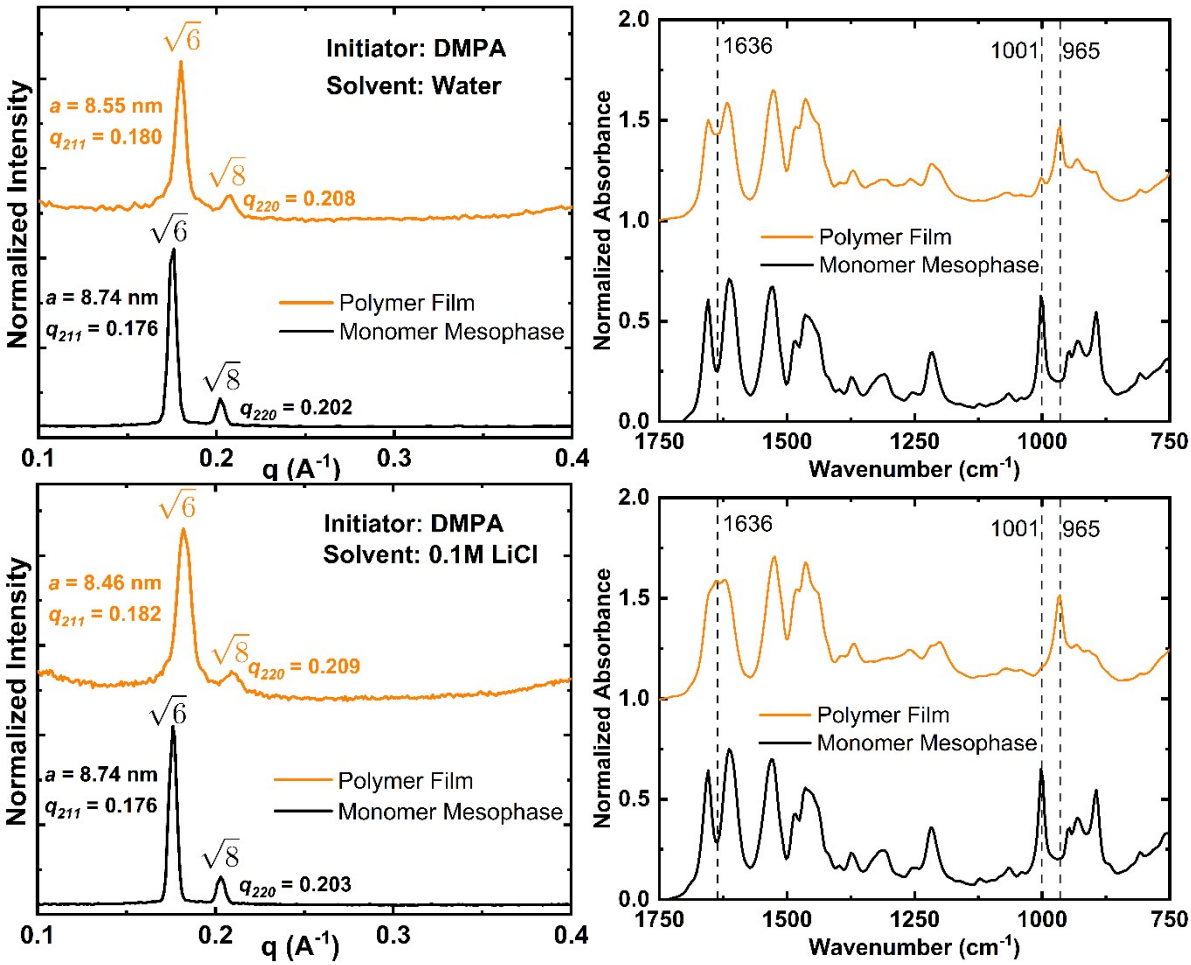

Fig. S8 SAXS and FTIR data for double-gyroid polymer films of **1** formulated with water and 0.1 M aq. LiCl, with 1 wt% DMPA initiator used for both solvents. For both solvents, FTIR spectra show that the diene tails exhibit quantitative conversion (disappearance of peak at 1001 cm^{-1} and appearance of a peak at 965 cm^{-1}). The polymer made from the 0.1 M aq. LiCl-based Q phase exhibits higher conversion of the methacrylamide headgroups (peak magnitude at 1636 cm^{-1}) than the corresponding water-based polymer material.

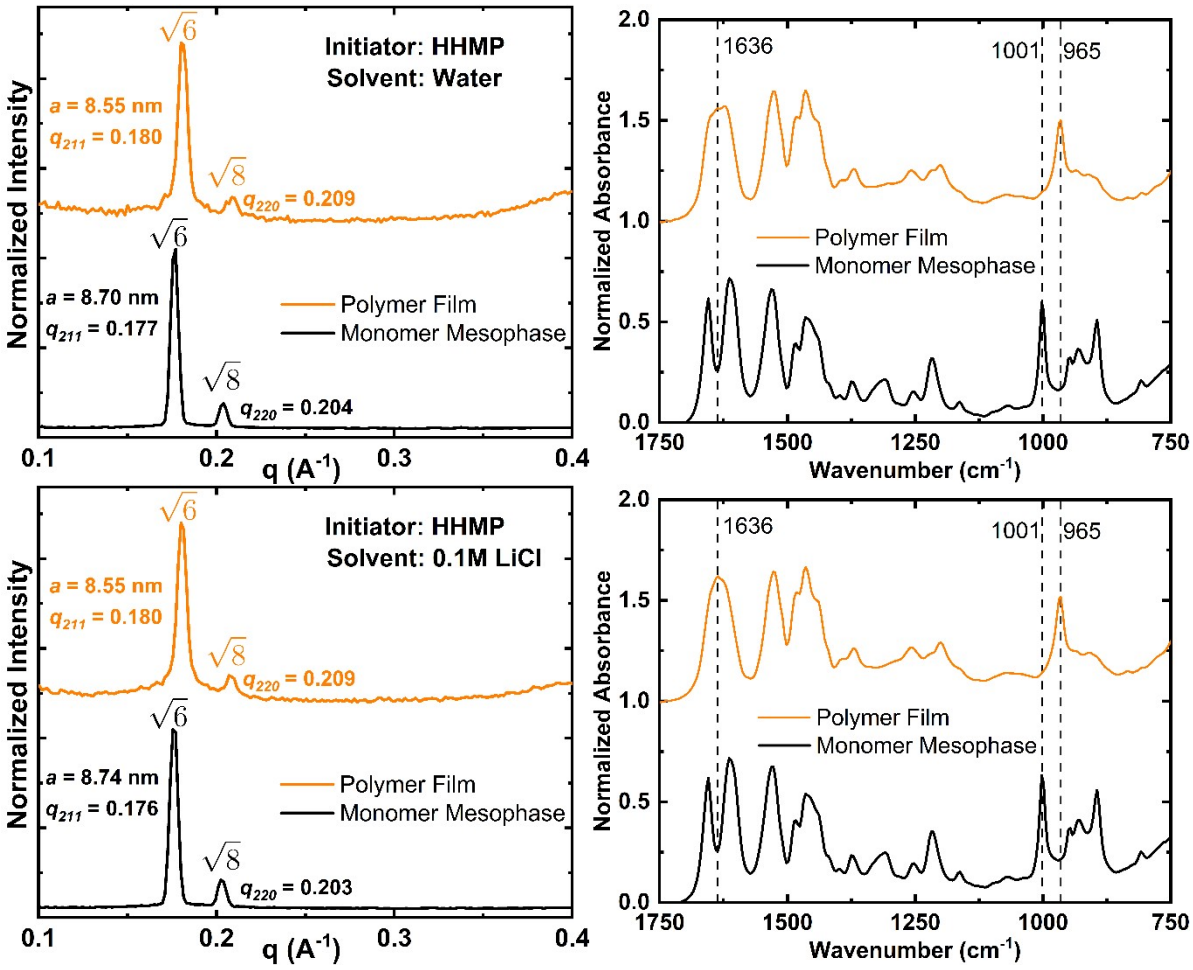

Fig. S9 SAXS and FTIR data for double-gyroid polymer films of **1** formulated with water and separately with 0.1 M aq. LiCl, with 1 wt% HHMP initiator used for both solvent systems. In both cases, the diene tail groups and methacrylamide headgroups show near-quantitative conversion in the FTIR spectra.

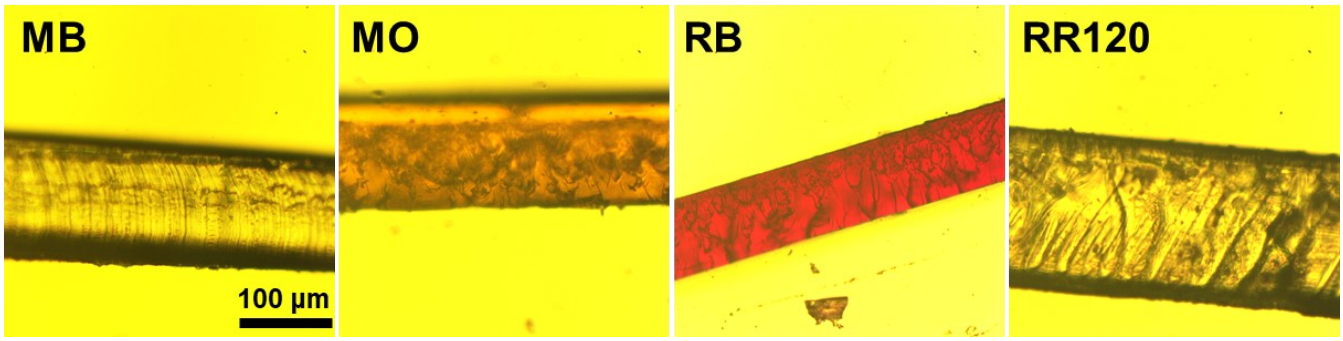

Fig. S10 Optical micrographs of cross-sections of the gyroid polymer films of **1** shown in Figure 4 of main manuscript. The absence of blue and red staining in MB and RR120 immersed films, respectively, indicates that the gyroid polymer pores are unable to adsorb those dyes in the film bulk due to charge and size exclusion mechanisms. Conversely, MO and RB dyes are fully infiltrated into the bulk of the gyroid films, providing additional evidence that the pore dimensions of the gyroid polymers are larger than the molecular sizes of those dyes.

Supplementary Calculations

Lipid and Water Domain Volume Fraction Calculation

Calculations of the water channel dimensions in a normal-type double-gyroid phase require estimates of lattice parameter *a* (obtained from SAXS), as well as volume fraction estimates for the lipid and water domains. We assume that the Br^- counterions associated with monomer **1** are present in the water channels. However, it is expected that Br^- ions are present near the pore walls; and further, that they act as 'hard spheres' to some degree, effectively constricting the pore dimension. To estimate this effect, in the subsequent calculations we include 50% of the Br^- volume fraction in the lipid volume ($\emptyset_{mem}$) and 50% in the water channel volume.

Table S2 Molecular weight and densities of monomer 1 components

	MW (Da)	Wt %	Density (g/mL)
Monomer 1 organic part	419.72	84	0.9 (assumed)
Monomer 1 Br^- ion	79.9	16	3.1

Table S3 Volume fraction calculations for various monomer 1 mesophase compositions

Mesophase	**H_I**	**Q_I**	**L**
***a* (nm)**	4.87	8.55	3.31
Monomer 1 (wt%)	70	88.5	93
Water (wt%)	30	11.5	7
Monomer 1 organic part (wt%)	58.8	74.34	78.1
Monomer 1 Br^- ion (wt%)	11.2	14.16	14.9
Monomer 1 organic part (vol%)	66	83.7	88.0
Monomer 1 Br^- ion (vol %)	3.7	4.6	4.9
Water (vol%)	30.3	11.7	7.1

Pore Diameter Calculation

Pore sizes within the *Ia3d* double-gyroid network were estimated from the approach outlined by Asghar et al. (Ref 27 in manuscript). First, the molecular volume *v* is estimated by using molecular weight (MW), density, and Avogadro's number. Here we only use the MW of the organic portion.

$$v = \frac{MW}{\rho N_{Avo}} = 0.775\ nm^3 \quad \text{(Eq. S.1)}$$

Next, the cross-sectional area of the molecule (at area-neutral surface within the lipid layer) A_n is calculated from the lattice parameter of the lamellar phase (a = 3.31 nm) and the volume fraction of the solid phase $\emptyset_{mem}$= 0.9045 (i.e., 0.88 + 0.049/2).

$$A_n = \frac{2v}{a_{lamellar}\emptyset_{mem}} = 0.5177\ nm^2 \quad \text{(Eq. S.2)}$$

Once the molecular parameter A_n (assumed to constant for all mesophases) is obtained, the radius r of surfactant cylinders in the H_I phase is calculated from the hexagonal phase lattice parameter (a = 4.87 nm) and volume fraction $\emptyset_{mem}$= 0.6785 (i.e., 0.66 + 0.037/2).

$$r = \sqrt{\frac{\sqrt{3}\emptyset_{mem}a_{hex}^{\ 2}}{2\pi}} = 2.106\ nm \quad \text{(Eq. S.3)}$$

The cross-sectional area per surfactant molecule at the surfactant-water interface, $A_{interface}$ is then estimated as

$$A_{interface} = \frac{2v}{r} = 0.7360\ nm^2 \quad \text{(Eq. S.4)}$$

Next, the molecular volume within the lipid bilayer corresponding to the area-neutral surface (assumed constant for all mesophases) is estimated as follows:

$$v_n = v\left(\frac{A_n}{A_{interface}}\right)^2 = 0.3834\ nm^3 \quad \text{(Eq. S.5)}$$

Lastly, the following implicit equation is used to calculate for z, which is the distance from the center of the water channel to area-neutral surface, by utilizing the geometric constants associated with *Ia3d* geometry (A_0 = 3.091, $\chi = -8$).

$$\frac{2A_0 a_{gyroid}^{\ 2}}{A_n}\left(1+\frac{2\pi\chi}{A_0 a_{gyroid}^{\ 2}}z^2\right)=\left[\frac{a_{gyroid}^{\ 3}-2A_0 a_{gyroid}^{\ 2} z\left(1+\frac{2\pi\chi}{3A_0 a_{gyroid}^{\ 2}}z^2\right)}{v_n}\right] \quad \text{(Eq. S.6)}$$

The value of *z* was calculated to be *z* = 0.78 nm. The value *z* represents an upper-bound for the water channel radius, assuming the area-neutral surface is found at the surfactant-water interface. Therefore, the upper bound for water channel diameter is 1.56 nm (i.e., 2 x 0.78 nm). If it is assumed that the area-neutral surface is found 1 to 2 carbons deeper in the solid layer than the surfactant-water interface, then *z* can be estimated as 0.65 nm, giving a pore diameter estimate of 1.3 nm.

Dye Size Calculations

The estimation of the molecular sizes is a complex and context dependent calculation. The geometric mean calculation procedure used here has many limitations, such as reporting an intermediate value between the longest and shortest dimensions of the molecule, which can obscure the effect of the 'controlling' molecular dimension. However, one advantage of the geometric mean lies in providing a single number for relative comparison purposes between variously shaped molecules (e.g., cylindrical Methyl Orange versus globular Vitamin B12). The additional utility provided by more accurate chemical size calculations can also be minimal when considering that molecular conformations can change in confined electrostatic pore environments.

Molecular dimensions reported in Figure 4 for the five dyes were calculated through ChemDraw and Chem3D software. The chemical structures of the respective dyes were first drawn in ChemDraw and then imported into Chem3D. The counter-ions were excluded from the chemical structures of dyes to simplify the size calculations and to avoid the software reporting of anomalous numbers. The molecular structure was aligned with the x-axis and centered on the origin using the corresponding commands in the View menu. Following this, an MM2 'Minimize Energy' simulation was performed on the molecules (except VB12) for 1000 iterations to obtain a molecular conformation with more realistic bond lengths and angles. Cartesian coordinates for all atoms were generated from the corresponding command in the Chem3D View menu. The table of Cartesian coordinates was then exported to Microsoft Excel. Following this, the range for each coordinate dimension was calculated from the coordinates of all molecules (i.e. $x_{max} - x_{min}$, y_{max}-y_{min}, and z_{max}-z_{min}). Lastly, the GEOMEAN command in Excel was used to calculated the geometric mean of the *x*,*y*, and *z* range. The obtained geometric mean value is reported as the effective dye size in the manuscript and Figure 4.

Table S4 Calculated molecular dimensions for various dyes

Dye	MW (Da)	$x_{max} - x_{min}$ (nm)	$y_{max} - y_{min}$ (nm)	$z_{max} - z_{min}$ (nm)	Geometric mean (nm)
Methyl Orange	327	1.373	0.544	0.312	0.615
Methylene Blue	320	1.379	0.227	0.551	0.557
Rose Bengal	974	0.710	1.000	1.085	0.916

Reactive Red 120	1469	1.893	1.404	1.748	1.668
Vitamin B12	1355	1.438	1.696	1.362	1.492

Specific Surface Area (SSA) Calculation

We employ two methods here to estimate the specific surface area (*S*) of the double-gyroid *Ia3d* network.

The first estimation technique is adapted from work by Detsi et al.[2] Assuming that the *Ia3d* unit cell consists of 2 pores and 2 solid ligaments, we can estimate the ligament size d_l from the SAXS obtained lattice parameter *a* and previously calculated pore diameter (d_p = *z*) as follows:

$$d_l = \frac{a}{2} - d_p = \frac{8.55}{2} - 1.56 = 2.715\ nm \qquad \text{(Eq. S.7)}$$

Next, the formula below (adapted from Equation 5 of ESI Ref. 2) is used to calculate *S* for the double-gyroid network, taking the value of dimensionless constant *C* = 5.8 and bulk density ρ = 1014 kg/m^3 (i.e., mass fraction weighted average of component densities in Table S2).

$$S = \frac{C}{\rho d_l}\left(\frac{d_l}{d_p}\right)^{-1} = 1210\,\frac{m^2}{g} \qquad \text{(Eq. S.8)}$$

An alternate estimate of the specific surface area can be obtained from the approach outlined by Ravikovitch and Neimark.[3] First, the reduced surface area per unit cell A_1 is estimated as follows (adapted from Equation 2 of ESI Ref. 3):

$$A_1 = A_0 + 2\pi\chi\left(\frac{d_l}{2a}\right)^2 = 1.825 \qquad \text{(Eq. S.9)}$$

Next, *S* is estimated from the equation below (adapted from Equation 6 of ESI Ref. 3).

$$S = \frac{2A_1}{\rho a \emptyset_{mem,gyroid}} = \frac{2(1.825)}{(1014)\left(8.55\times10^{-9}\right)(0.86)} = 490\,\frac{m^2}{g} \qquad \text{(Eq. S.10)}$$

We note that both expressions for *S* follow essentially the same functional form, and differ primarily in the value of the constant employed. The actual value of *S* is likely closer to the lower estimate (i.e., 490 m^2 g^{-1}).

The estimates for *S* can also be used to roughly estimate the adsorption capacity of the gyroid polymers. Using the lower *S* estimate, the surface-area-per-headgroup A_n (Eq. S2), and Avogadro's number, an estimated n_{sites} for the number/moles of positively charged quaternary ammonium sites per mass of gyroid polymer is obtained:

$$n_{sites} = \frac{S}{A_n N_{Avo}} = \frac{490}{\left(5.18\times10^{-19}\right)\left(6.022\times10^{23}\right)} = 1.6\times10^{-3}\frac{mol}{g} \qquad \text{(Eq. S.11)}$$

Combining the above calculation with the absorption data in Figure 4, the masses of immersed polymer films, and an assumed 1:1 binding site ratio between dye molecule: quaternary ammonium headgroup, we can estimate the adsorption capacity used up by the dye uptake reported in Figure 4 of the manuscript.

For example, for the MO dye solution (V_{MO} = 40 mL, c_{MO} = 15 µmol/L, abs_{MO} = 90% absorption @ 72 hrs), the immersed polymer film had a mass m_{film} = 6.0 mg, leading to:

$$Used\ Adsorption\ Capacity = \frac{V_{MO}c_{MO}abs_{MO}}{n_{sites}m_{film}} = 0.057 = 5.7\ \% \quad \text{(Eq. S.12)}$$

The above estimate can also be repeated for the RB dye (V_{MO} = 40 mL, c_{MO} = 15 µmol/L, abs_{MO} = 55% absorption @ 72 h, m_{film} = 5.0 mg), leading to an estimate for 4.2% used capacity. These estimates indicate that most likely the actual equilibrium absorption capacity of the gyroid polymers is much higher than the measured adsorption numbers at the 72-h mark for MO (29 mg/g or 90 µmol/g) and RB (64 mg/g or 66 µmol/g) dyes.

It should be noted that the above calculations are rough estimates, and can be performed with different assumptions to obtain different estimates. For instance, for the estimated surface area per headgroup, $A_{interface}$ (Eq. S4) can be used instead of A_n (Eq. S2). Similarly, for adsorption capacity estimates, the larger estimate of S (1210 m^2/g) can be utilized. Given that the RB dye molecule has 2 negatively charged sites, the adsorption capacity of the polymer films can be estimated differently by assuming a 1:2 dye molecule: quaternary ammonium headgroup ratio. Additional complexities not addressed by these rough estimates include the relative geometric confinement of dye molecules within the channel dimensions disrupting perfect monolayer formation, and the possibility of progressively slower diffusion deeper into the bulk of the gyroid polymer film.

Finally, the areal density σ of quaternary ammonium species at the water interface can be used with an assumption regarding stoichiometry of the dye based on electrostatic interactions (e.g., 1 RB per 2 quaternary ammonium sites) to arrive at an estimate for the adsorption capacity. Functionally this is related to the estimate above for n_{sites}, but it uses the estimate of the ligament size d_l as the starting point. For a lamellar sheet of thickness t the volume per unit area is $t/2$ as there are two surfaces and the mass is $m = t\rho/2$ where ρ is the density of the polymer sheet.

The number of groups at the surface per unit area is then the product of the number of groups per molecule ($g_m =$ 1 quaternary ammonium), the number of molecules per unit thickness of the sheet ($m_s =$ 2, due to bilayer arrangement), the mass $t\rho$, and Avogadro's number, divided by the molar mass of the molecules. Here, with 499.6 the molar mass of monomer 1, the estimated

$$\sigma_{LAM}\sigma = \frac{g_m m_s m}{M} N_{Avo} = \frac{t\rho}{M} N_{Avo} = 3.2\ nm^{-2} \quad \text{(Eq. S.13)}$$

For cylinders of diameter D, $m = \frac{\rho D}{4}$ and the areal density is given by a similar expression, reduced by a factor of 2

$$\sigma_{CYL} = \frac{D\rho}{2M} N_{Avo} = 1.6\ nm^{-2} \quad \text{(Eq. S.14)}$$

For completeness, for spheres, per unit area, the mass is $m = \frac{\rho D}{6}$ and the corresponding expression for areal density of sites is

$$\sigma_{SPH} = \frac{D\rho}{3M} N_{Avo} \quad \text{(Eq. S.15)}$$

If we use the geometric mean of the LAM and CYL results to approximate the expected areal density for a gyroid surface, we yield 2.3 nm^{-2}. This number agrees reasonably well with the expected areal density of roughly 2 nm^{-2} based on $\sigma_{GYR} = 1/A_n$.

We can estimate the absorption capacity n_{sites} now as

$$\sigma_{SPH} n_{sites} = \frac{S\,\sigma}{N_{Avo}} = \frac{(490)(2.3 \times 10^{18})}{(6.022 \times 10^{23})} = 1.9 \times 10^{-3} \frac{mol}{g} \quad \text{(Eq. S.16)}$$

References for the ESI

1. B. A. Pindzola, J. Jin and D. L. Gin, *J. Am. Chem. Soc.* 2003, **125**, 2940.
2. E. Detsi, E. De Jong, A. Zinchenko, Z. Vukovic, I.Vukovic, S. Punzhin, K. Loos, G. ten Brinke, H. A. De Raedt, P. R. Onck, J. T. M. De Hosson, *Acta Mater.* 2011, **59**, 7488.
3. P. I. Ravikovitch and A. V. Neimark, *Langmuir*, 2000, **16**, 2419.